Solar Energy 221 (2021) 232–242

Contents lists available at ScienceDirect

Solar Energy

journal homepage: www.elsevier.com/locate/solener

Photovoltaic modules transient response analysis and correction under a fast characterization system

Eneko Ortega *, Gerardo Aranguren, Juan Carlos Jimeno

Technological Institute of Microelectronics, University of the Basque Country (UPV/EHU), 48013 Bilbao, Spain

ARTICLE INFO

Keywords:
Photovoltaic systems
Monitoring
Fault detection
Capacitive load
Hysteresis effect

ABSTRACT

Failures of single photovoltaic (PV) modules lead to significant power losses in large PV systems. Individual and periodic monitoring of each PV module is a powerful way to detect these losses. Recently, a novel monitoring method, named Module to Module Monitoring System (M3S), has been proposed. This monitoring method, without disconnecting the PV module from the rest of the system, is able to produce and measure small variations around the operating point of the PV module. The entire measurement is performed in less than 5 ms, using only low-power components. For current high-efficiency PV modules, these short measurement times generate a hysteresis effect in the current–voltage (I-V) curve during the transient-state, which makes it difficult to directly estimate the static I-V characteristics of the PV module. In this work, the transient response of the PV module is analyzed and a methodology to correct the hysteresis effect and estimate the I-V characteristics is implemented. From the obtained dynamic measurements, the proposed methodology is able to estimate the I-V characteristics of the PV module around the operating point with a mean squared error below 0.8%.

1. Introduction

Solar photovoltaic (PV) is currently one of the fastest growing energy source. By 2019, installed PV capacity increased to more than 600 GW (Louwen and van Sark, 2020) and it is expected to grow by more than 140 GW in 2020. Most of this new PV capacity will be installed in large PV systems with hundreds of thousands of PV modules. Thermal losses, DC/AC conversion losses, wiring losses and failures in PV modules and in the rest of the system, among others, result in power losses of approximately 15–20% of the performance ratio (Khalid et al., 2016; Matsumoto et al., 2016).

PV module power losses due to degradation typically increase by around 0.6% per year (Jordan et al., 2016). In addition, PV modules failures (Buerhop et al., 2018; Cristaldi et al., 2015; Dhimish et al., 2018; Silverman et al., 2016; Sinha et al., 2018), may increase power losses and speed up this degradation rate (Köntges et al., 2016). Extreme weather conditions such as hailstorms (Muehleisen et al., 2018) or hurricanes (Hotchkiss and Walker, 2020) also have a severe impact on PV system performance. Moreover, a failure on a single module may lead to a higher power loss since PV modules are connected to each other. Thus, the automatic and periodic monitoring of PV systems is of major importance.

Several monitoring methods have been proposed to detect these failures. Some of these approaches measure electrical data at string level or at the inverter entry (Bright et al., 2018; Silvestre et al., 2016; Wang et al., 2018). However, it is not clear if this methods are able of detecting failures on single PV modules (Jones et al., 2018; Ortega et al., 2017) since these failures may be diluted among the entire system. At module level, some methods measure the operating voltage of the module (Jones et al., 2018; Kilper et al., 2015) or the output power (Han et al., 2015; Samara and Natsheh, 2019). However, with these methods its not always possible to detect the fault or to indentify which is the failing module. For that, better access to the current–voltage (I-V) curve of each module is required. I-V curve tracers measure the full I-V curve of the PV module (Belmili et al., 2010; Duran et al., 2007; Spertino et al., 2015), characterizing the PV module. These methods require to disconnect the PV module from the rest of the system, long measuring times and power electronics components and large capacitors.

Due to these limitations, in (Ortega et al., 2019) a new methodology named Module to Module Monitoring System (M3S) was proposed. M3S, without power electronics components and with capacitors in the range of tens of microfarads, is able to take partial measurements of the I-V curve. These measurements are taken in a few milliseconds without disconnecting the PV module under measurement from the rest of the

* Corresponding author.
E-mail address: eneko.ortegam@ehu.eus (E. Ortega).

https://doi.org/10.1016/j.solener.2021.03.032
Received 14 July 2020; Received in revised form 3 November 2020; Accepted 14 March 2021
Available online 4 May 2021

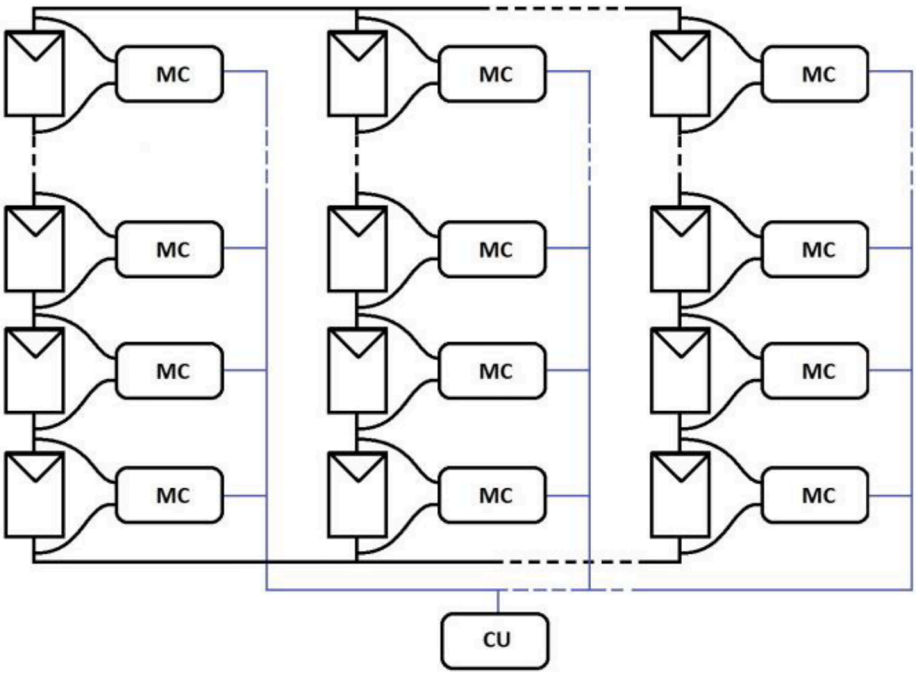

Fig. 1. Monitoring methodology for a PV system, with one monitoring circuit (MC) for each PV module and a control unit (CU) for the entire system.

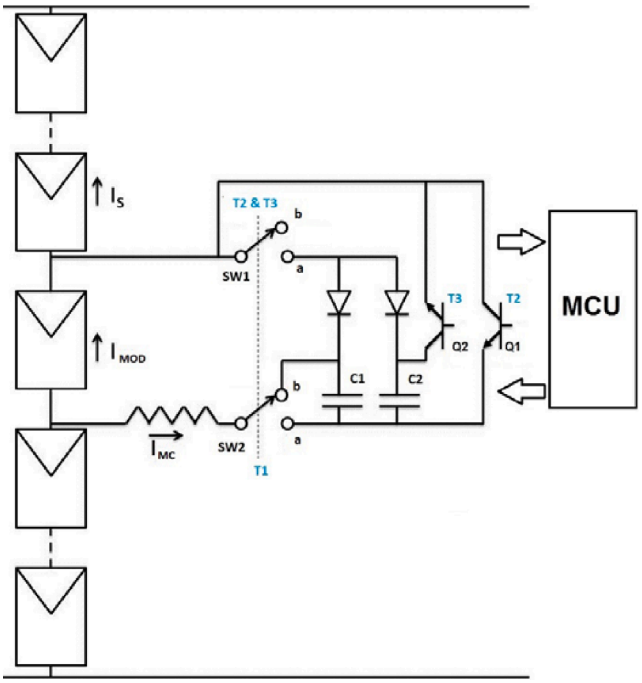

Fig. 2. Monitoring circuit (MC) simplified scheme connected to a single PV module on a string. The MC is based on two small capacitors (C1 and C2), four transistors (SW1, SW2, Q1 and Q2) controlled by a microcontroller and two diodes controlled by the current.

system. This proposal was evaluated in a low-capacitance 25 W PV module, and an accuracy of between 1 and 3% was achieved when recomposing the I-V characteristics for the region close to the maximum power. However, the I-V characteristic estimation of a state-of-the-art PV module, with higher minority carrier lifetimes, connected in a string is not as straightforward. Due to the dynamic response of the PV modules and the interaction with the rest of the system, further processing is required to estimate the I-V characteristics. The aim of this work is to analyze the dynamic response of PV modules when measured using the M3S, a fast characterization system, and to present a correction method for the dynamic effects caused by internal associated capacitances.

2. Description of the system

This monitoring methodology, which has been explained in detail in previous work (Ortega et al., 2019) can be implemented on any system size. However, it is intended for central inverter systems, where there are hundreds of PV modules for each inverter and there is little information about each PV module. The monitoring methodology is based on two different circuits, one control unit (CU) for the entire PV system and a monitoring circuit (MC) connected in parallel to each PV module. Fig. 1 shows the proposed monitoring system for an entire PV system. Each MC is able to measure its PV module automatically and remotely and send the measurement data to the CU, which performs the further processing.

The simplified scheme of the MC is shown in Fig. 2. The MC is a low cost electronic circuit that uses only low-power components and is able to disturb the operating point of the PV module by modifying its output current. The MC is based on two 22 μF capacitors controlled by six switches: four switches (transistors: Q1, Q2, SW1 and SW2) controlled by an 8-bit microcontroller and another two (diodes) controlled by the direction of the current.

The MC, has four operating modes: standby, T1, T2 and T3. Most of the time, the MC is in standby mode and no current is extracted from the PV module. During T1, the first step of the monitoring sequence, capacitors C1 and C2 are charged in a slow process (50 ms) to the module voltage, draining little current from it. In T2, capacitor C1 is discharged towards the PV module, increasing the output current of the module with a step-like function limited to 0.3 A. This way, the operating point is displaced towards short-circuit. This movement is done outside the static I-V characteristics since, due to the intrinsic capacitance of PV modules, the dynamic behavior is not able to follow the PV module I-V characteristics. Once the capacitor is discharged, it returns to the initial operating point with values similar to those of the static I-V characteristics, since the movement is much slower. During T3 the operating point is displaced to higher voltages through capacitors C1 and C2, decreasing

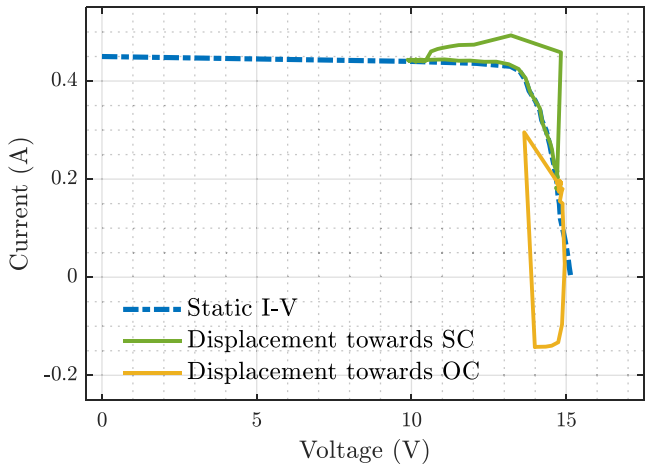

Fig. 3. Measurement with the MC in a 25 W PV module. Static I-V characteristics (dashed blue line), displacement towards short-circuit (SC) (green line, T2) and displacement towards open-circuit (OC) (yellow line, T3).

the output current in 0.3 A and moving it to open-circuit with a similar behavior to T2. Once the operating point returns again to equilibrium, the MC switches back to standby mode. During T2 and T3, which are completed in a few milliseconds, the MC takes pairs of current and voltage values with a 35 μs sampling period and sends them to the CU.

The MC has been previously evaluated with a 25 W Isofotón bifacial PV module following the described setup in (Ortega et al., 2019). The results obtained are shown in Fig. 3. The green line shows the movement of the operating point to short-circuit (T2) and the yellow line indicates the movement to open-circuit (T3). The T2 and T3 sequences take only 3 ms each to be completed. From these data, based on the methodology explained on the previous paper, it is possible to recompose the I-V characteristics of the 25 W PV module with an accuracy between 1 and 3% for the region close to the maximum power. A final version of the MC could be integrated, except for the two capacitors, on a single integrated circuit including in that the communications system, which could be done through Power Line Communications (PLC) or other communication system. The MC could be integrated in each PV module with a cost in the dollar range.

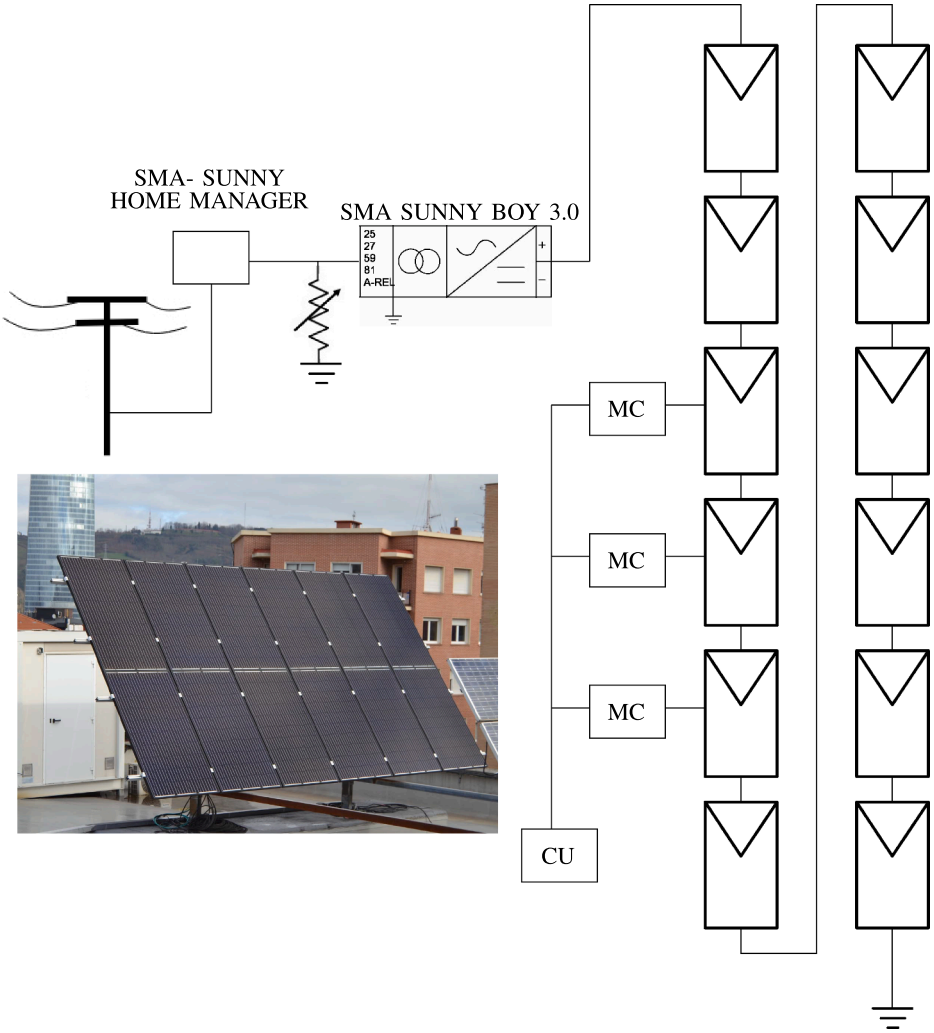

Fig. 4. 3.42 kW PV system setup. The figure shows the MC connected to three of the PV modules and the CU connected to them. At the bottom left, the 12 modules are shown.

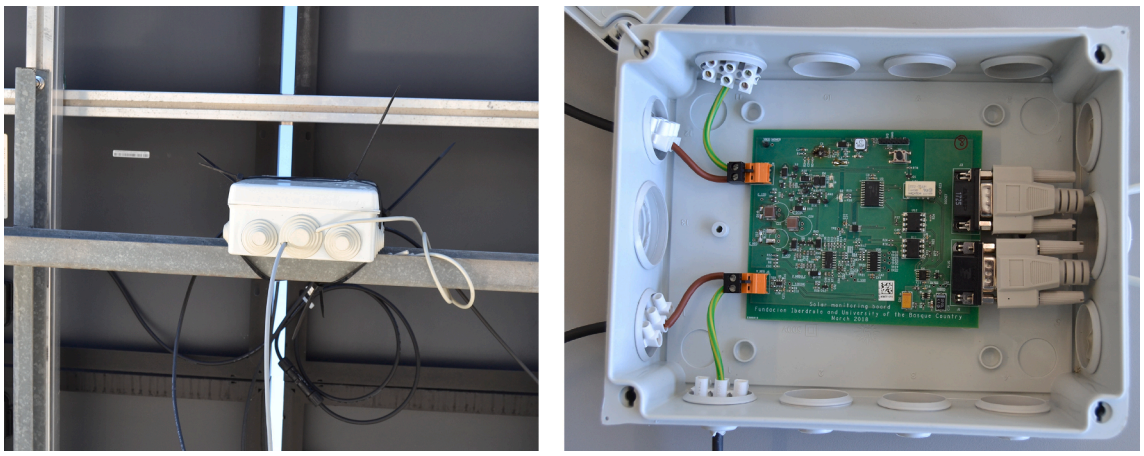

Fig. 5. Monitoring circuit (MC) attached to the rear side of the second PV module of the string.

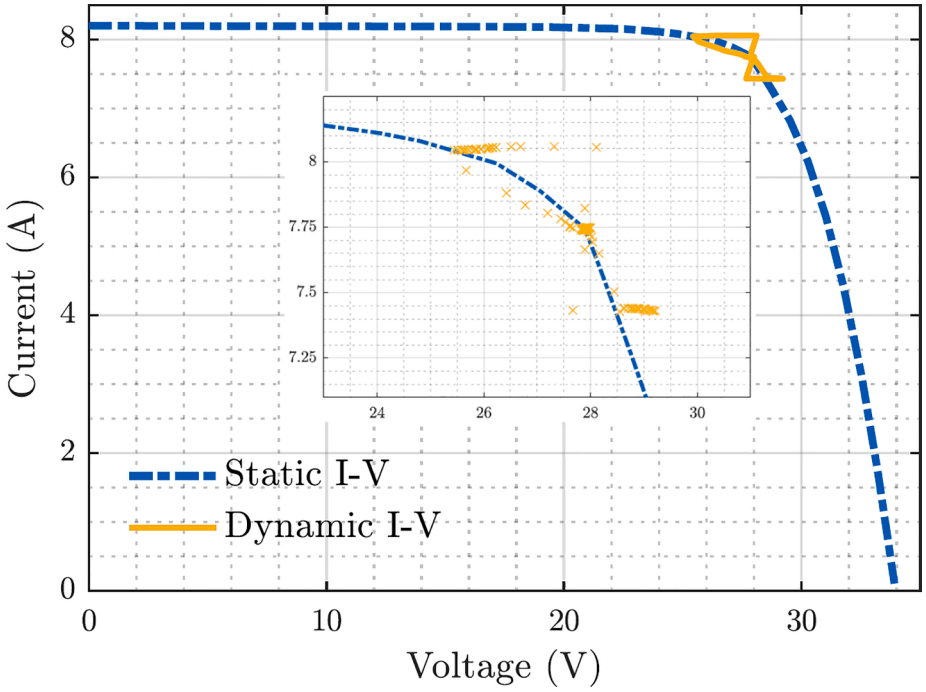

Fig. 6. Measurement with the MC in a 285 W PV module. Static I-V characteristics (dashed blue line) and dynamic I-V characteristics (yellow line).

3. Dynamic considerations

As stated in the introduction section, in low-capacitance PV modules is easy to directly estimate the I-V characteristic with this method and it has been already demonstrated. However, in PV modules with higher minority carriers lifetimes is not as straightforward. This section intends to address this aspect. For that, the monitoring methodology has also been evaluated in a state-of-the-art high efficiency PV module, with longer response times. For that purpose, the setup shown in Fig. 4 has been implemented on the roof of the Faculty of Engineering in Bilbao (Spain). The 3.42 kW PV system is composed of 12 monocrystalline Jinko JKMS285M-60 PV modules (Jinko Solar, Shanghai, China) connected in series and a SMA-Sunny Boy 3000TL-21 inverter (SMA, Niestetal, Germany). The inverter is connected to a variable load and to an SMA-Sunny Home Manager, which allows controlling the injected power to the grid and thus, adjusting the operating point of the system, testing the monitoring methodology at different operating points. These 285 W modules have, under standard test conditions (STC), $V_{oc} = 38.7\text{V}, I_{sc} = 9.51\text{A}$ and an efficiency of 17.41% (19.5% at the cell level). The MC is connected in parallel to the PV module and strapped to the rear side of the PV module as shown in Fig. 5. In (Ortega et al., 2019) preliminary results with this PV system were presented, obtaining a dynamic I-V curve equivalent to the previous curve obtained with the 25 W module.

Fig. 6 shows the dynamic I-V characteristics (yellow line) obtained with the MC in the 285 W module during normal operation, without disconnecting it from the rest of the system, and the static I-V curve (dashed blue line).

Static I-V data was obtained measuring current and voltage values of the PV module, under a small number (6) of different loads, and fitting the measured points to a PV module which includes a current generator, a diode and series and shunt resistances, as the typical one diode model. Measured points were fitted to the I-V curve using the Multiv software (Martinez and Jimeno, 1998). Dynamic I-V data, on the other hand, was measured with the methodology explained in Section 2, during PV modules normal operation, with the MC connected in parallel to the PV module as shown in Fig. 5. In the subsequent analyses, static I-V curve is used as a reference to determine the accuracy of the dynamic data.

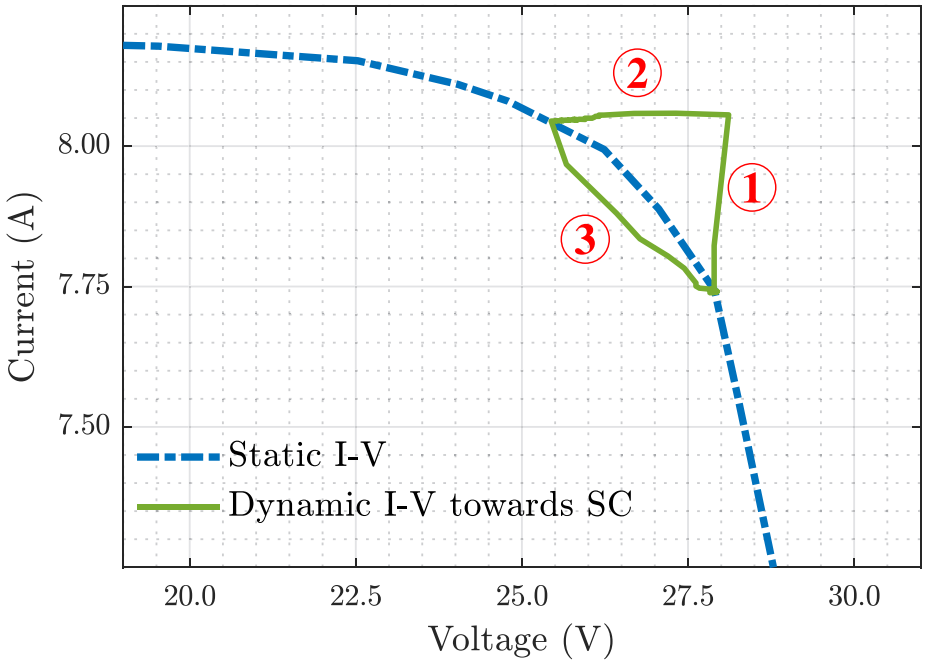

Fig. 7. Displacement towards short-circuit with the MC in a 285 W PV module. Static I-V characteristics (dashed blue line) and dynamic I-V characteristics (green line). Three sections can be identified: one, shift of the operating point; two, discharge of the capacitor; and 3, return to equilibrium.

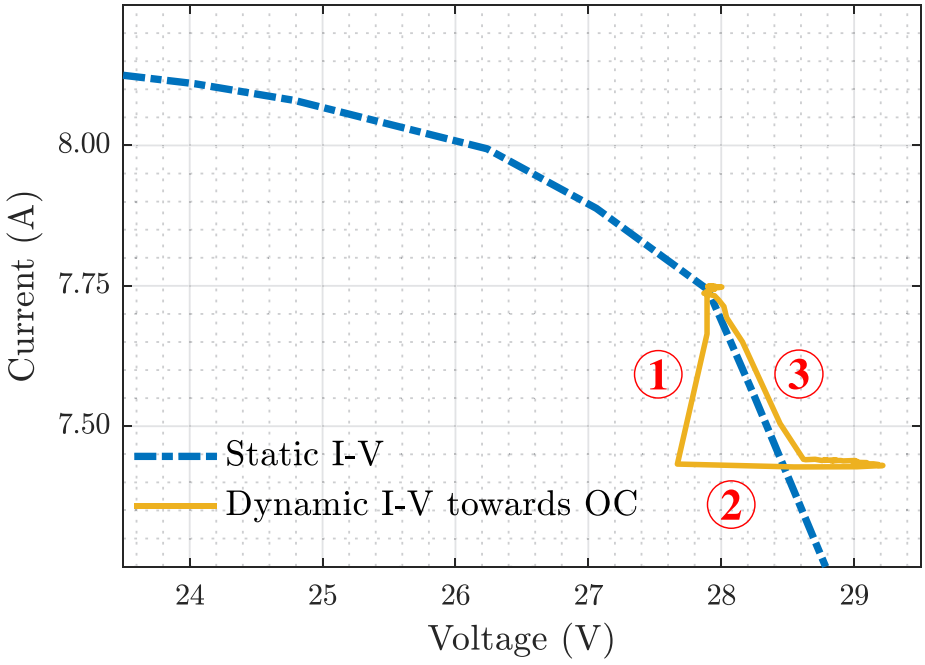

Fig. 8. Displacement towards open-circuit with the MC in a Jinko JKMS285-60 PV module. Static I-V characteristics (dashed blue line) and dynamic I-V characteristics (yellow line). Three sections can be identified: one, shift of the operating point; two, discharge of the capacitor; and 3, return to equilibrium.

In this experiment, the MC is able to move the operating point, for the current operating point, 3 V to short-circuit and 2 V to open-circuit, but always the voltage sweep is limited by the 0.3 A current step. Fig. 6 also shows a zoom of the operating point area with the sample points of the acquired data. These points show how the rate of change of the operating point is not constant during the measurement. The measurement shows a high sample density near the operating point and maximum deviation points and a lower sample density in intermediate areas. In Figs. 7 and 8 a detailed zoom of the displacement of the operating point towards short-circuit and open-circuit is shown. Similar to the results obtained with the 25 W module (Ortega et al., 2019), in both measurements three sections can be identified: the shift of the operating point (Section 1) with a sudden current increase or decrease as a function of the displacement direction, the discharge of the capacitor (Section 2) and the return to the operating point (Section 3). However, there are some differences with the 25 W PV module. For the 285 W PV module, the return path (Section 3) is not close to the static I-V characteristics of the PV module. This result is due to the higher efficiency of state-of-the-art PV modules (in this experiment, the 285 W PV modules) than the efficiency of the 1980s small PV module such as the Isofoton's

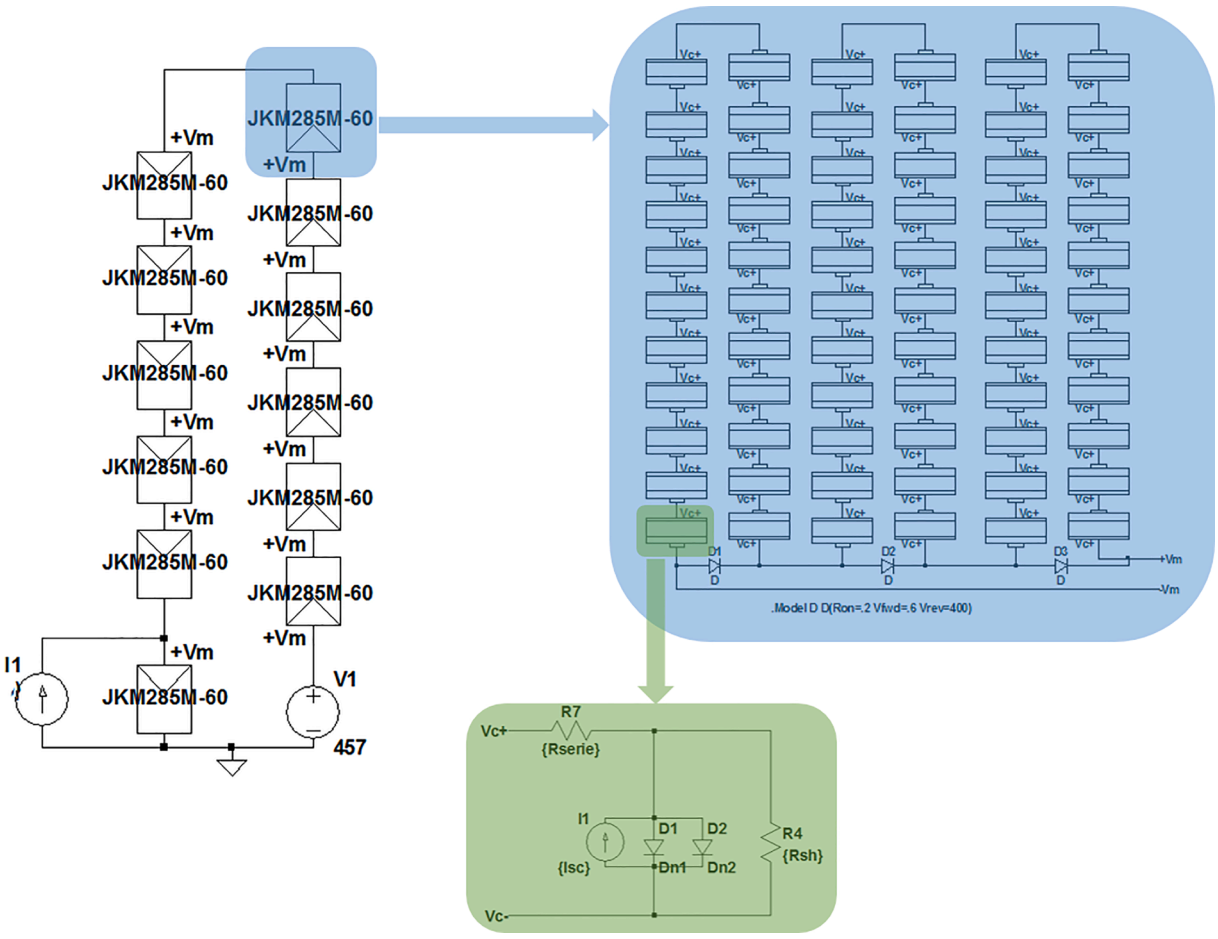

Fig. 9. Model of the 3.42 kW PV system with 12 Jinko JKMS285M-60 PV modules developed with LTspice IV.

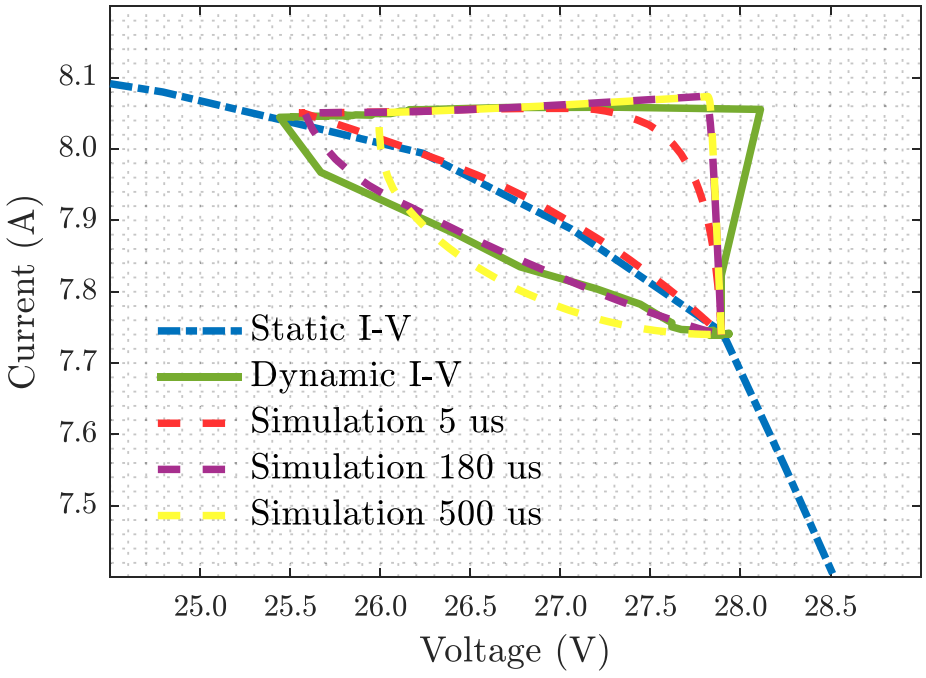

Fig. 10. Simulation transient-states for three different PV cell response times: 5 μs (red), 180 μs (purple) and 500 μs (brown). The static I-V curve (blue) matches the 5 μs response time, and the 285 W PV module dynamic I-V curve (green) matches the 180 μs response time.

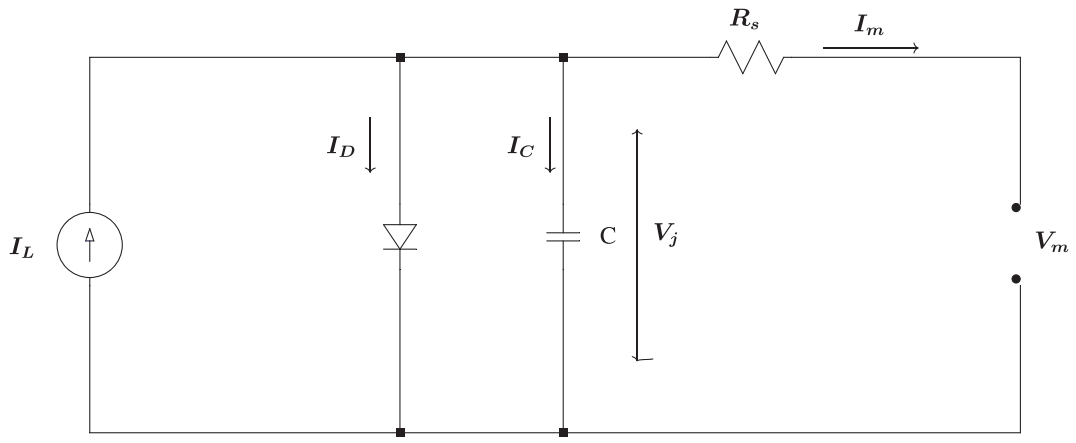

Fig. 11. Single diode model PV module equivalent circuit.

bifacial 25 W module.

As the efficiency of the module increases, the effective carrier lifetime increases, with a larger internal associated capacitance and longer response times. This means that an abrupt change in applied illumination or current implies a delayed change in the PV module voltage. This effect is observed for any PV module, but it increases as the PV cell response time increases. When measuring with the proposed monitoring methodology, this associated capacitance generates transient artifacts in the obtained values. In the reverse (REV) direction (movement towards short-circuit, Section 1 and 2 in Fig. 7 and Section 3 in Fig. 8) the measured current is higher than the static current since the internal capacitance is charging. Conversely, in the forward (FW) direction (movement towards open-circuit, Section 3 in Fig. 7 and Section 1 and 2 in Fig. 8) the current values are smaller than the static current since the internal capacitance is discharging (Monokroussos et al., 2006; Edler et al., 2012).

In order to verify that the hysteresis loop of Figs. 7 and 8 is due to the PV module dynamic, the experimental results are confirmed on a simulation environment. The MC is a small but complex electronic circuit whose dynamic behavior, how it interacts with the PV module and with the rest of the system is unknown. It is not clear if the obtained hysteresis loop is only due to the dynamic behavior of the PV module or if; in addition, there is an interaction with the MC dynamic and with the rest of the modules.

Fig. 9 shows the model of the 3.42 kW PV system implemented on LTspice IV (Linear Technology, California, United States). Each PV cell is modeled with the double-diode model and the simulation environment enables the modification of its parameters. One of the diodes is a dynamic diode, through their internal transit-time parameter, enables to simulate several minority carrier lifetimes. The model of the PV system is composed of 12 PV modules, one of them with a current source connected in parallel. The MC is a complex circuit but it can be simulated with a step-like current injection of -0.3 A for 2 ms, which increases the module output current by 0.3 A and moves its operating point towards short-circuit. The behavior of the PV module with several response times between 5 μs and 500 μs is analyzed. The PV system is simulated at 0.9 suns and a cell temperature of 43 °C to be coincident with the actual conditions of the module under test.

Fig. 10 shows the static I-V curve, for the movement towards short-circuit, the experimental results on the 285 W PV module and the simulation results for three different response times. For the simulation curves, as the cell response time increases, the output current of the PV module decreases in the FW direction, returning to the operating point along a more distant path from the static I-V curve. For PV modules with fast response times (5 μs), the simulation presents a return path very close to the static I-V characteristics, in line with the experimental results obtained with the 25 W PV module (Ortega et al., 2019). From this dynamic curve, it is possible to directly estimate the static I-V curve, with an error below 3%. For longer response times (180 μs), a more severe hysteresis effect is observed due to higher internal associated capacitances. This finding is in line with the experimental results obtained on the 285 W PV modules (green). For these response times, the FW path is far from the static I-V curve, and it is not possible to directly estimate it. For longer response times (500 μs), the hysteresis effect is even larger. This effect has also been experimentally confirmed adding an external capacitance to the 25 W module (Ortega et al., 2018), obtaining a larger hysteresis loop. These results confirm that the hysteresis effect observed during fast measurement of PV modules with the MC, depends on the PV cell response times and it is not significantly affected by the MC dynamic behavior or by its interaction with the rest of the system.

This hysteresis effect during fast I-V curve measurement of PV modules is a well known problem and appears for two main reasons: the I-V curve scanning speed and the scanning direction. Several methods have been proposed to minimize the occurrence of the hysteresis effect using different voltage profiles (Ferretti et al., 2013; Monokroussos et al., 2012; Virtuani et al., 2012) or multi-flash (Sinton et al., 2005) or long pulse (Hu et al., 2011) in the case of use of flash measurements. A minimum of 500 ms flash pulses are used in many cases to measure PV modules (Hishikawa et al., 2013; Ramspeck et al., 2014). Accordingly, different parameters optimization approaches have been proposed to determine the optimum scanning time or the minimum number of points, among others, to minimize the hysteresis effect (Gao et al., 2018; Herman et al., 2012). Other approaches propose a correction method for fast I-V curve measurements based on a slow measurement of the dark I-V curve (Kojima et al., 2014; Virtuani and Rigamonti, 2013).

Recently, a new approach was proposed (Sinton et al., 2017) to correct the hysteresis effect in PV cells or modules. This method is based on estimating the dynamic capacitance of the PV module from a weighted sum of the forward and reverse currents and then determining the capacitive current of the PV module. By adding this current to the forward or reverse current, it is possible to approximate the I-V characteristics of the PV module. This proposal has already been implemented for PV cell I-V measurements, using solar simulators (Vahlman et al., 2018), with a minimum sweep time between 20 and 30 ms.

According to the PV module equivalent circuit in Fig. 11, the total current of the PV module (I_m) can be given as the sum of the steady-state current and dynamic current, as in Eq. (1). Steady-state currents comprise the photogeneration current (I_L) and the recombination current (I_D). The dynamic or capacitive current (I_c) is due to the charge and discharge of PV module solar cells during voltage sweeps.

$$\mathrm{I}_m = \mathrm{I}_L - \mathrm{I}_D - \mathrm{I}_c. \tag{1}$$

During steady-state conditions, while there is no voltage variation, I_c

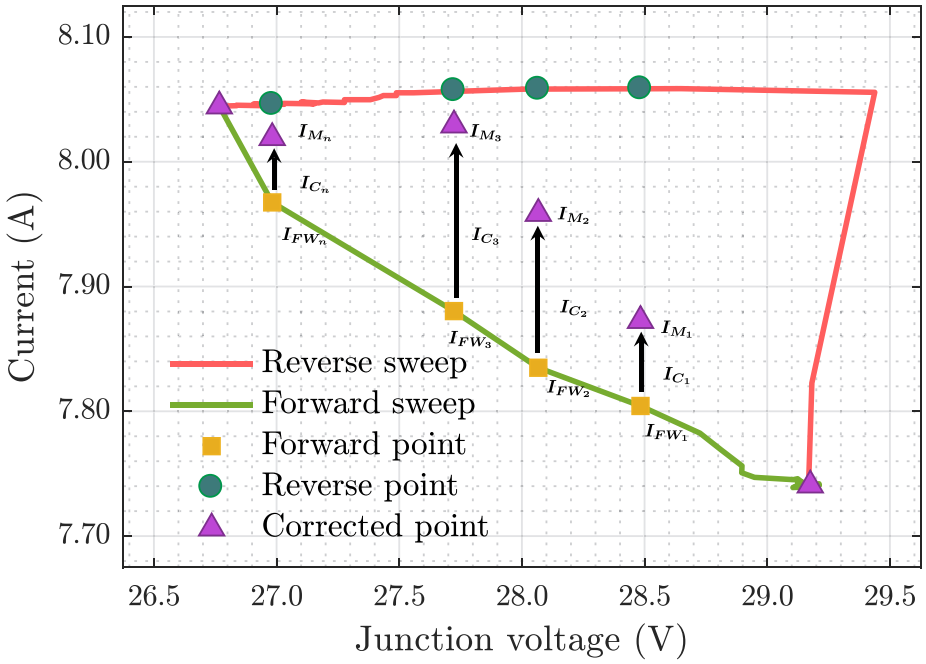

Fig. 12. Forward (green line) and reverse (red line) sweeps for the movement towards short-circuit given at junction voltage. Yellow squares (FW points), green circles (REV points), purple triangles (corrected points) and black arrows depict the correction process. From I_{FW_i}, adding $I_{c_i\|FW}, I_{M_i}$ is obtained from Eq. (5).

is zero and the module current depends only on I_L and I_D. Variations from steady-state current during the transient-state are due to changes in the capacitive current (Kerr et al., 2002), which according to Eq. (2) depends on the voltage and its rate of change:

$$\mathrm{I}_c = \mathrm{C}(\mathrm{V}_j)\cdot\frac{\mathrm{dV}_j}{\mathrm{dt}}. \tag{2}$$

where V_j is the junction voltage and can be computed as:

$$\mathrm{V}_j = \mathrm{R}_s\cdot\mathrm{I}_m + \mathrm{V}_m. \tag{3}$$

From there, the FW and REV currents can be subtracted, and the capacitance of the PV module can be estimated as:

$$\mathrm{C}(V_j) = \frac{\mathrm{I}_{m,REV}(V_j) - \mathrm{I}_{m,FW}(V_j)}{\left.\frac{\mathrm{dV}_j}{\mathrm{dt}}\right|_{FW} - \left.\frac{\mathrm{dV}_j}{\mathrm{dt}}\right|_{REV}} \tag{4}$$

Knowing the PV module capacitance, the module current can be corrected as:

$$\mathrm{I}_m(V_j) = \mathrm{I}_{m,FW}(V_j) + \mathrm{C}(V_j)\left.\frac{\mathrm{dV}_j}{\mathrm{dt}}\right|_{FW} \tag{5}$$

Even if this method is able to estimate the steady-state I-V

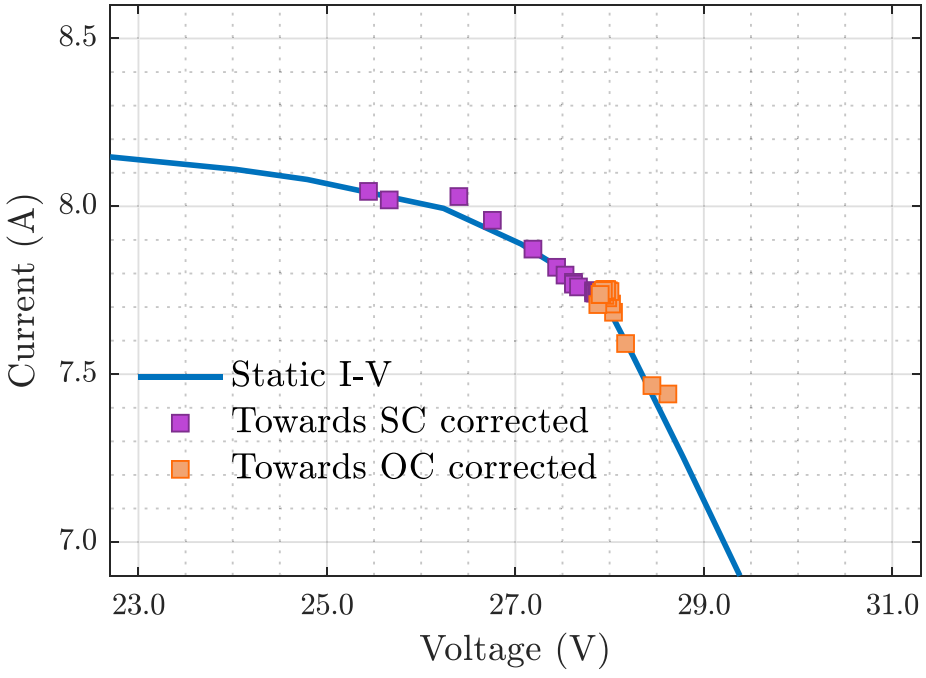

Fig. 13. Static I-V characteristic (blue), corrected points from the short-circuit sweep (purple) and corrected points from he open-circuit sweep (orange).

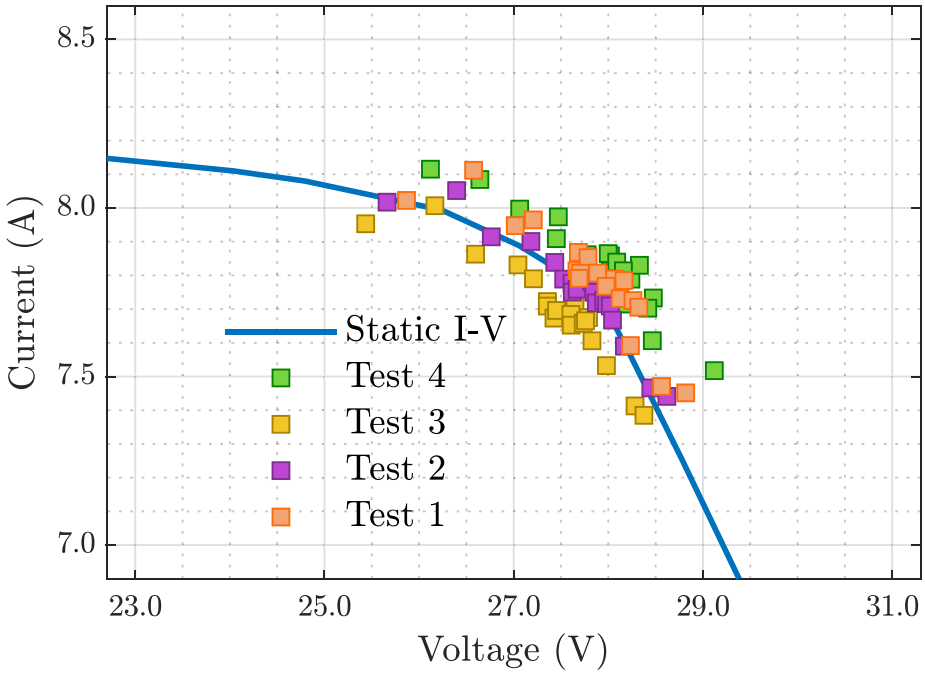

Fig. 14. Static I-V characteristic (blue) and corrected points (towards short-circuit and open-circuit) for four test on the same module and under the same operating conditions.

characteristics of the PV module from two dynamic measures, it has two general constraints (Vahlman et al., 2018): at least 20–30 ms long voltage sweeps have been advised in each direction to ensure enough accuracy for I-V curve estimation, and it has two possible noise sources. At cell level, the correction method would be very sensitive to the series resistance determination accuracy, especially with short voltage sweeps. In addition, the time derivative of the junction voltage is very sensitive to measurement data error.

When applied to the data acquired from the MC, there are other specific limitations: first, with M3S, only a small section of the I-V curve (around the operating point) is known. I-V curve tracers, typically measure the full I-V curve two times: from V_{oc} to I_{sc} and from I_{sc} to V_{oc}. M3S, however, only measures a small segment of the I-V characteristics around the operating point in each direction (steps T2 and T3 of the monitoring sequence). Each measurement is divide into two parts: the movement from the operating point to the maximum deviation point, and the return to the operating point. In this way, if we consider the measurement towards short-circuit (step T2), the movement from the operating point towards short-circuit would be the REV sweep and, the return to the operating point would be the FW sweep.

Second, the measurement is very fast, an order of magnitude shorter than the advised time. Step T2, taking into account the REV and FW sweeps, takes only 3 ms to be completed (Ortega et al., 2019). Finally, the FW and REV sweeps are typically made with known voltage profiles, obtaining current values at the same voltage in the forward and reverse directions, which are necessary to estimate the capacitance value according to Eq. (4). In this proposal, because the movement is generated by a current injection with the charge and discharge of a capacitor, as explained in Section 2, and data are acquired with an 8-bit microcontroller, the sampling frequency is constant; however, since the rate of change of the voltage is not constant, samples are obtained at different voltages in the FW and REV directions. Therefore, before implementing this method, the FW and REV samples require to be synchronized, which adds an additional error to the process.

The displacement towards short-circuit (Fig. 7) is chosen to implement this correction method with M3S, with Sections 1 and 2 being the REV direction and Section 3 being the FW direction. From these data, the forward and reverse points are changed from module voltage to junction voltage using Eq. (3), with $R_s = 0.165\,\Omega$. R_s was estimated from the three-parameter model of the PV module, where from I_{sc}, V_{oc} and FF manufacturer data there is only one R_s value that fits the model. Small variations in R_s value have no influence on the method accuracy. Fig. 12 shows the reverse (red) and forward (green) sweeps. For both sweeps, the V_j derivative is computed and, since there are very few samples and any acquisition error could lead to a much higher derivative error, the derivative is fitted to a second order polynomial expression. From Eq. (4) the module mean capacitance is determined, obtaining a value of 32 μF. With this value, from Eq. (5), the adjusted module current for the movement towards short-circuit (T2) is computed by adding the FW and capacitance currents. This way, as shown in Fig. 12, for each FW point the corrected current of the module (I_{M_i}) can be estimated by adding to the FW current (I_{FW_i}) at that point the capacitance current ($I_{c_i\|FW}$). The process show in Fig. 12 is repeated for the entire sweep. Similarly, the same process is repeated for the movement towards open-circuit (step T3, Fig. 8, Section 3), correcting the I-V curve by adding the capacitance and REV currents.

Fig. 13 shows the fitting between the steady-state I-V curve and the adjusted I-V points in both directions: short-circuit (purple points) and open-circuit (orange points). The proposed correction methodology shows good fitting with the steady-state I-V curve around the operating point. A mean squared error (MSE) of 0.33% is obtained between the corrected points and the static I-V curve points. However, in particular points (e.g. 26.3 V in the curve from Fig. 13) the relative error increases to 0.7%. Without the polynomial fitting of the voltage derivative the error would be more than 1.2%. With the few points obtained from the MC, this method is able to estimate the I-V characteristics of the PV module around maximum power point with error values under 0.33%. In addition, unlike when applying at cell level, this methodology is very insensitive to R_s determination accuracy. A R_s value 20 times greater than the used one would only increase the MSE from 0.33% to 0.38%.

Several tests have been performed on the same module, in a short period of time, following the same process. Fig. 14 shows the fitting between the corrected points and the static I-V curve for four tests, after applying the proposed methodology. As it can be seen, the corrected points show good fitting with the static I-V curve. Observed deviations between tests can be due to small variations on the operating point. For

Table 1
For three modules of the PV system: MSE between static and dynamic I-V characteristic, static and dynamic MPP and error between them. For each PV module, four measures were performed. Static MPP variations between modules are due to operating conditions variations during the experiments.

Module number	MSE (mean ± std) (%)	Static MPP (W)	Dynamic MPP (mean ± std) (W)	Maximum error (%)
1	0.43 ± 0.12	216.03	217.80 ± 2.11	1.41
2	0.51 ± 0.21	160.51	159.64 ± 2.18	2.05
3	0.41 ± 0.09	185.36	185.72 ± 1.42	0.97

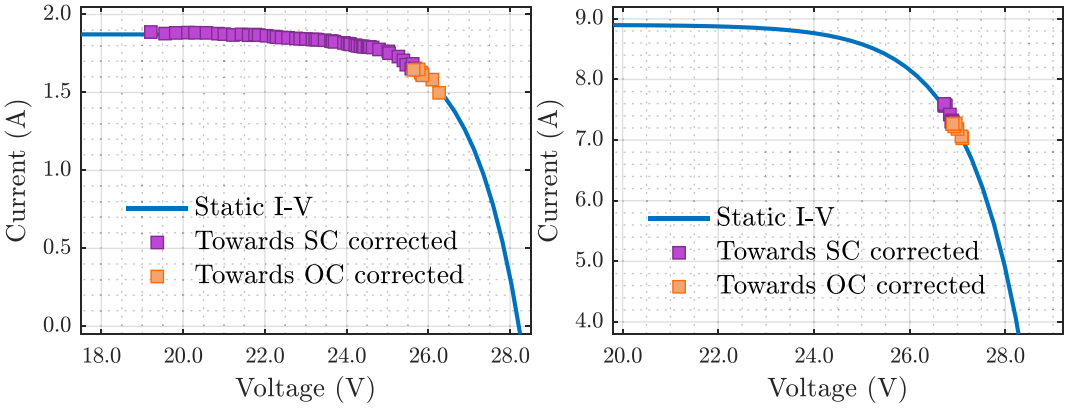

Fig. 15. Correction method at two tests: with low illumination (left) and closer to open-circuit (right). Static I-V characteristic (blue), corrected points from sweep towards short-circuit (purple) and corrected points from sweep towards open circuit (orange).

all the tests, the error remains low, with an MSE (mean ± standard deviation) of 0.43 ± 0.12%.

To evaluate the proposed methodology on different modules, the same process has been repeated for three of the modules, connecting the MC in parallel to them (Fig. 4). Firstly, the static I-V characteristic is obtained for each of the modules as previously explained. Then, four measures are performed for each PV module and dynamic data is corrected with the proposed methodology. Finally, the MSE between static and dynamic data and the maximum error between static and dynamic maximum power point (MPP) is computed. Table 1 shows these results. Even if some error is added due to operating conditions variation while performing the measurements, for all the modules and all the tests the I-V characteristic around MPP is estimated with an MSE below 0.8% and the MPP is estimated with a maximum error below 2.1%.

Finally, Fig. 15 shows two tests at two particular conditions. At the left side, on a cloudy day, with low illumination, which obtained an MSE of 0.51%. At the right side, on an operating point closer to open-circuit, which obtained an MSE of 0.57%. Even for measures like this two, at more extreme conditions, the proposed methodology is able to estimate the I-V characteristic of the PV module around the operating point with an error below 0.8%.

These results are obtained even though the measures are performed in times as short as 5 ms for both directions and some error is added during processing due to the need to estimate the reverse voltage points.

4. Conclusions

The dynamic response of a current state-of-the-art PV module connected within a string, when measured using M3S, a fast characterization system, has been analyzed.

The monitoring system, using only low-power components and small capacitors, is able to produce and measure small variations around the operating point of the PV module during normal operation. The monitoring process is done remotely and the entire measurement is performed in less than 5 ms.

Such fast measurements generate a hysteresis effect in the obtained dynamic I-V curve. The simulation results show that the hysteresis effect is related to solar cell effective lifetime. Fast response modules, generate a dynamic I-V curve very close to the static curve. As the effective lifetime increases, the current of the FW sweep decreases, returning through a path farther from the static I-V curve. Experimental measurements are in line with these results.

An algorithm based on computing a weighted sum of the FW and REV currents to estimate the corrected I-V curve of the PV modules has been implemented. Even if only a small segment of the I-V curve is measured and the sweep time is an order of magnitude shorter than the advised times, the implemented method obtains an MSE below 0.8% when estimating the static I-V curve around the operating point. In addition, when estimating the MPP, the error remains below the 2.1%.

The proposed methodology shows good results in order to estimate the static I-V characteristic around MPP and to estimate the MPP of the module. However, there is no information of the rest of the I-V characteristic. For that, mathematical processing must be expanded to obtain a better recomposition of the full I-V characteristic of the PV module, estimate its parameters (I_{sc}, V_{oc}, I_{01} …) and determine the failure causes.

Declaration of Competing Interest

The authors declare that they have no known competing financial interests or personal relationships that could have appeared to influence the work reported in this paper.

Acknowledgements

This work was supported by the Basque Country Government [Grant No. PRE_2016_1_0016] and [project Promise Elkartek 19/49]; and the Fundación Iberdrola España [Convocatoria de ayudas a la Investigación en Energía y Medio Ambiente 2018].

References

Belmili, H., Cheikh, S.M.A., Haddadi, M., Larbes, C., 2010. Design and development of a data acquisition system for photovoltaic modules characterization. Renewable Energy 35, 1484–1492.

Bright, J.M., Killinger, S., Lingfors, D., Engerer, N.A., 2018. Improved satellite-derived pv power nowcasting using real-time power data from reference pv systems. Sol. Energy 168, 118–139.

Buerhop, C., Wirsching, S., Bemm, A., Pickel, T., Hohmann, P., Nieß, M., Vodermayer, C., Huber, A., Glück, B., Mergheim, J., et al., 2018. Evolution of cell cracks in pv-modules under field and laboratory conditions. Prog. Photovoltaics Res. Appl. 26, 261–272.

Cristaldi, L., Faifer, M., Lazzaroni, M., Khalil, M.M.A.F., Catelani, M., Ciani, L., 2015. Diagnostic architecture: A procedure based on the analysis of the failure causes applied to photovoltaic plants. Measurement 67, 99–107.

Dhimish, M., Mather, P., Holmes, V., 2018. Evaluating power loss and performance ratio of hot-spotted photovoltaic modules. IEEE Trans. Electron Devices 65, 5419–5427.
Duran, E., Galán, J., Sidrach-de Cardona, M., Andujar, J., 2007. A new application of the buck-boost-derived converters to obtain the IV curve of photovoltaic modules. In: 2007 IEEE Power Electronics Specialists Conference. IEEE, pp. 413–417.
Edler, A., Schlemmer, M., Ranzmeyer, J., Harney, R., 2012. Understanding and overcoming the influence of capacitance effects on the measurement of high efficiency silicon solar cells. Energy Procedia 27, 267–272.
Ferretti, N., Pelet, Y., Berghold, J., Fakhfouri, V., Grunow, P., 2013. Performance testing of high-efficient pv modules using single 10 ms flash pulses. In: 28th European Photovoltaic Solar Energy Conference, Paris, France, pp. 3184–3187.
Gao, Q., Zhang, Y., Yu, Y., Meng, F., Liu, Z., 2018. Effects of i–v measurement parameters on the hysteresis effect and optimization in high-capacitance pv module testing. IEEE J. Photovolt. 8, 710–718.
Han, J., Lee, I., Kim, S.H., 2015. User-friendly monitoring system for residential PV system based on low-cost power line communication. IEEE Trans. Consum. Electron. 61, 175–180.
Herman, M., Jankovec, M., Topič, M., 2012. Optimal iv curve scan time of solar cells and modules in light of irradiance level. Int. J. Photoenergy 2012.
Hishikawa, Y., Shimura, H., Tobita, H., 2013. Accurate iv curve measurements of high-capacity c-si solar cells: Effects of iv testers and new technology for rapid measurement. In: Proc. 28th Eur. Photovoltaic Sol. Energy Conf., pp. 3159–3161.
Hotchkiss, E.L., Walker, H., 2020. Observations of PV Systems Post-Hurricane. Technical Report. National Renewable Energy Lab. (NREL), Golden, CO (United States).
Hu, B., Li, B., Zhao, R., Yang, T., 2011. Reflection-type single long-pulse solar simulator for high-efficiency crystalline silicon photovoltaic modules. Rev. Sci. Instrum. 82, 065104.
Jones, C.B., Ellis, B.H., Stein, J.S., Walters, J., 2018. Comparative review of high resolution monitoring versus standard inverter data acquisition for a single photovoltaic power plant. In: 2018 IEEE 7th World Conference on Photovoltaic Energy Conversion (WCPEC)(A Joint Conference of 45th IEEE PVSC, 28th PVSEC & 34th EU PVSEC), pp. 0715–0720.
Jordan, D.C., Kurtz, S.R., VanSant, K., Newmiller, J., 2016. Compendium of photovoltaic degradation rates. Prog. Photovoltaics Res. Appl. 24, 978–989.
Kerr, M.J., Cuevas, A., Sinton, R.A., 2002. Generalized analysis of quasi-steady-state and transient decay open circuit voltage measurements. J. Appl. Phys. 91, 399–404.
Khalid, A.M., Mitra, I., Warmuth, W., Schacht, V., 2016. Performance ratio–crucial parameter for grid connected PV plants. Renew. Sustain. Energy Rev. 65, 1139–1158.
Kilper, T., Kruse, I., Feser, I., Kirstein, U., Peters, D., 2015. A new generation of PV monitoring system with high-grade remote diagnostic based on module level monitoring and integrated yield simulation. In: 31st European Photovoltaic Solar Energy Conference and Exhibition (EU PVSC 2015), pp. 1679–1682.
Kojima, H., Iwamoto, K., Shimono, A., Abe, J., Hishikawa, Y., 2014. Accurate and rapid measurement of high-capacitance pv cells and modules using a single short pulse light. In: 2014 IEEE 40th Photovoltaic Specialist Conference (PVSC). IEEE, pp. 1896–1898.
Köntges, M., Altmann, S., Heimberg, T., Jahn, U., Berger, K.A., 2016. Mean degradation rates in pv systems for various kinds of pv module failures. In: Proc. of the 32nd European Photovoltaic Solar Energy Conference and Exhibition, München: WIP, pp. 1435–1443.
Louwen, A., van Sark, W., 2020. Photovoltaic solar energy. In: Technological Learning in the Transition to a Low-Carbon Energy System. Elsevier, pp. 65–86.
Martinez, V., Jimeno, J., 1998. Simultaneous fit to I-V characteristics of solar cells. In: Second World Conference and Exhibition on Photovoltaics Solar Energy Conversion.
Matsumoto, Y., Norberto, C., Urbano, J.A., Ortega, M., Asomoza, R., 2016. Three-year PV system performance in Mexico City. In: 2016 IEEE 43rd Photovoltaic Specialists Conference (PVSC). IEEE, pp. 3168–3172.
Monokroussos, C., Etienne, D., Morita, K., Dreier, C., Therhaag, U., Herrmann, W., 2012. Accurate power measurements of high capacitance pv modules with short pulse simulators in a single flash. In: Proc. 27th Eur. Photovolt. Sol. Energy Conf., pp. 3687–3692.
Monokroussos, C., Gottschalg, R., Tiwari, A., Friesen, G., Chianese, D., Mau, S., 2006. The effects of solar cell capacitance on calibration accuracy when using a flash simulator. In: 2006 IEEE 4th World Conference on Photovoltaic Energy Conference. IEEE, pp. 2231–2234.
Muehleisen, W., Eder, G.C., Voronko, Y., Spielberger, M., Sonnleitner, H., Knoebl, K., Ebner, R., Ujvari, G., Hirschl, C., 2018. Outdoor detection and visualization of hailstorm damages of photovoltaic plants. Renewable energy 118, 138–145.
Ortega, E., Aranguren, G., Jimeno, J.C., 2019. New monitoring method to characterize individual modules in large photovoltaic systems. Sol. Energy 193, 906–914.
Ortega, E., Aranguren, G., Saenz, M., Gutierrez, R., Jimeno, J., 2017. Study of photovoltaic systems monitoring methods. In: Photovoltaic Specialists Conference (PVSC).
Ortega, E., Aranguren, G., Saenz, M., Gutierrez, R., Jimeno, J., 2018. Photovoltaic module to module monitoring system. In: 2018 IEEE 7th World Conference on Photovoltaic Energy Conversion (WCPEC)(A Joint Conference of 45th IEEE PVSC, 28th PVSEC & 34th EU PVSEC), IEEE, pp. 2703–2708.
Ramspeck, K., Schenk, S., Komp, L., Metz, A., Meixner, M., 2014. Accurate efficiency measurements on very high efficiency silicon solar cells using pulsed light sources. In: Proc. 29th Eur. Photovolt. Sol. Energy Conf. Exhib., pp. 1253–1256.
Samara, S., Natsheh, E., 2019. Intellingent real-time photovoltaic panel monitoring system using artificial neural networks. IEEE Access 7, 50287–50299.
Silverman, T.J., Mansfield, L., Repins, I., Kurtz, S., 2016. Damage in monolithic thin-film photovoltaic modules due to partial shade. IEEE J. Photovolt. 6, 1333–1338.
Silvestre, S., Mora-López, L., Kichou, S., Sánchez-Pacheco, F., Dominguez-Pumar, M., 2016. Remote supervision and fault detection on OPC monitored PV systems. Sol. Energy 137, 424–433.
Sinha, A., Pore, S., Balasubramaniyan, A., TamizhMani, G., 2018. Acceleration factor modeling for degradation rate prediction of photovoltaic encapsulant discoloration. In: 2018 IEEE 7th World Conference on Photovoltaic Energy Conversion (WCPEC)(A Joint Conference of 45th IEEE PVSC, 28th PVSEC & 34th EU PVSEC), IEEE, pp. 1342–1346.
Sinton, R.A., De Ceuster, D., Wilson, K., Barbosa, L.R., 2005. Flash testing high-efficiency silicon solar cells and modules. In: Proc. 20th European Photovoltaic Energy Conf., Barcelona, Spain, pp. 659–662.
Sinton, R.A., Wilterdink, H.W., Blum, A.L., 2017. Assessing transient measurement errors for high-efficiency silicon solar cells and modules. IEEE J. Photovolt. 7, 1591–1595.
Spertino, F., Ahmad, J., Ciocia, A., Di Leo, P., Murtaza, A.F., Chiaberge, M., 2015. Capacitor charging method for I-V curve tracer and MPPT in photovoltaic systems. Sol. Energy 119, 461–473.
Vahlman, H., Liping, J., Hyvarinen, J., Tolvanen, A., Hyvarinen, S., 2018. Capacitive effects in high-efficiency sola cells duing i–v curve measurement: Considerations on error of correction and extraction of minority carrier lifetime. In: 35st European Photovoltaic Solar Energy Conference and Exhibition (EU PVSC 2018), pp. 254–261.
Virtuani, A., Rigamonti, G., 2013. Performance testing of high-efficient highly-capacitive c-si pv modules using slow-speed dark current-voltage characteristics and a reconstruction procedure. In: Proc. 28th Eur. Photovoltaic Sol. Energy Conf., pp. 2876–2881.
Virtuani, A., Rigamonti, G., Friesen, G., Chianese, D., Beljean, P., 2012. Fast and accurate methods for the performance testing of highly-efficient c-si photovoltaic modules using a 10 ms single-pulse solar simulator and customized voltage profiles. Meas. Sci. Technol. 23, 115604.
Wang, J.Y., Qian, Z., Zareipour, H., Wood, D., 2018. Performance assessment of photovoltaic modules based on daily energy generation estimation. Energy 165, 1160–1172.